Kusumah, Ferdi Perdana; Kyyrä, Jorma

Initial Current Injection Method of a Direct Three-Phase to Single-Phase AC/AC Converter for Inductive Charger

Published in:
Proceedings of the 2018 International Power Electronics Conference, IPEC-Niigata - ECCE Asia 2018

DOI:
10.23919/IPEC.2018.8507417

Published: 22/10/2018

Document Version
Peer-reviewed accepted author manuscript, also known as Final accepted manuscript or Post-print

Please cite the original version:
Kusumah, F. P., & Kyyrä, J. (2018). Initial Current Injection Method of a Direct Three-Phase to Single-Phase AC/AC Converter for Inductive Charger. In *Proceedings of the 2018 International Power Electronics Conference, IPEC-Niigata - ECCE Asia 2018* (pp. 3870-3876). Article 8507417 (International Conference on Power Electronics). IEEE. https://doi.org/10.23919/IPEC.2018.8507417

Initial Current Injection Method of a Direct Three-Phase to Single-Phase AC/AC Converter for Inductive Charger

Ferdi Perdana Kusumah* and Jorma Kyyrä
Department of Electrical Engineering and Automation
School of Electrical Engineering
AALTO UNIVERSITY
P.O. Box 13000
FI-00076 Aalto, Finland
URL: http://eea.aalto.fi/en/
*E-mail: ferdi.kusumah@aalto.fi

***Abstract*—This paper explains an initial current injection method of a direct three-phase to single-phase AC/AC converter for an inductive charger. The converter has a lesser number of switches than a matrix converter and uses a resonant circuit to utilize zero-current switching. The method applies a DC resonant charging to charge a primary resonant capacitor, by taking advantage of the converter topology. The charged voltage is used to boost the initial current since in practice an affordable current transducer has only a limited measurement range, due to its accuracy and noise characteristics. The method is applied to kick-start the inductive charger without adding an amplification circuit to the current transducer output. Simulation results are presented to verify theoretical calculations.**

Keywords*—AC/AC converter, battery charger, contactless power supply, resonant converter.

I. Introduction

A concept of an inductive-based contactless power transfer (ICPT) for an electric vehicle charger has been introduced in [1], [2] and [3]. It incorporates a direct three-phase to single-phase AC/AC converter connected to a resonant circuit. The converter topology has a lesser number of bi-directional switches than a matrix converter and a similarity to the one given in [4] and [5], with an added advantage of using Zero-current switching (ZCS) mechanism through injection and free-wheeling oscillation commutations previously introduced in [6], [7] and [8]. The ZCS operation forces the converter to always monitor primary resonant current characteristics which are amplitude and zero-crossings.

However in practice, an affordable current transducer only has a limited measurement capability. For example, a CASR-6 transducer that has a maximum measurement range of ± 20 A and output voltage range of 0.375-4.625 V, will have a difficulty in measuring ± 2.5 A, since the output voltage only corresponds to 2.125 ± 0.266 V [9]. An output voltage amplification can be applied to increase the measurement range. But noise is usually present in practical case that can also be amplified and further corrupts the results [10]. Due to the limitations, practical current oscillation during initial transient of the AC/AC converter with a limited input source voltage amplitude cannot be monitored properly. This leads to a difficulty in switching the converter at the state, since its operation is based on current zero-crossings.

A method to boost initial current amplitude will be studied in this paper. It is based on a DC resonant charging principle to charge a primary resonant capacitor, by taking advantage of the converter topology [10] [11]. Capacitor voltage after charging can produce a sufficient current amplitude for the current transducer, where its output will be used to operate the AC/AC converter switches.

This paper is organized as follows. A brief explanation of a direct AC/AC converter topology and its operation is given in Section II. Section III gives explanation on the charging method and its mathematical model. In Section IV, simulation results obtained from PLECS software are presented to verify the initial injection method. Finally, conclusions of the paper are given in the last section.

II. System Description

A. Circuit explanation

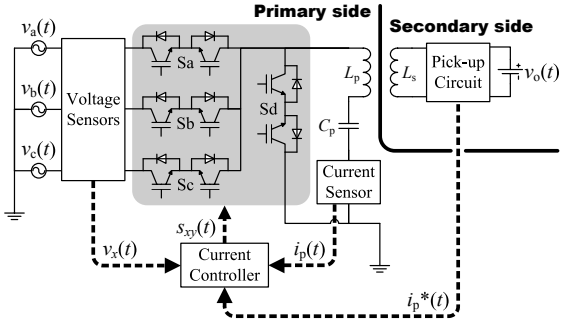

Fig. 1: ICPT system schematic. Grey area highlights bi-directional switches arrangement of the direct AC/AC converter.

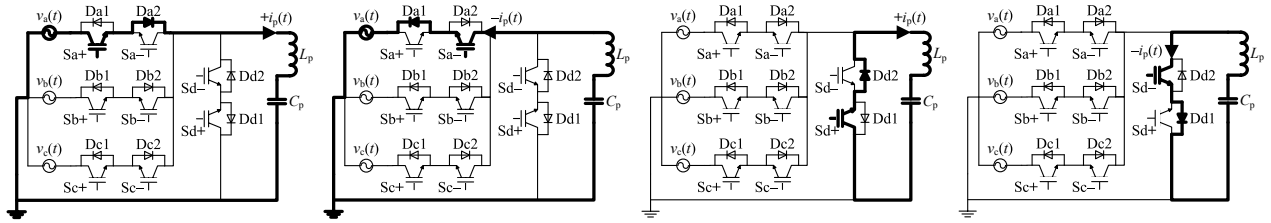

Fig. 2: Commutation modes of a direct AC/AC converter. Sub-figure (a) and (b) illustrate injection mode, while (c) and (d) show free-wheeling oscillation commutation. A clock-wise current flow is defined as a positive flow.

A schematic of the ICPT system is given in Fig. 1. The switching topology consists of three pair of bi-directional switches Sa, Sb and Sc connected to a three-phase power source and has a common connection to a resonant circuit L_p and C_p. The Sd switch pair is used as a free-wheeling path of primary current. An on-off current controller is utilized to produce gate signals $s_{\mathrm{xy}}(t)$ for managing converter output power. The power management is achieved through controlling primary current amplitude. The controller uses voltage $v_\mathrm{x}(t)$ and current $i_\mathrm{p}(t)$ information, obtained from corresponding sensors. It also accepts current reference signal, which is $i_\mathrm{p}^*(t)$ from the secondary pick-up circuit. The primary and secondary sides are magnetically coupled and the pick-up circuit contains a rectifier, a DC/DC converter, and a battery equipped with a voltage sensor [1].

The AC/AC converter has two types of commutation which are injection and free-wheeling oscillation as illustrated in Fig. 2. In injection mode, the current goes either from the three-phase source to the resonant circuit or vice versa, while during free-wheeling, the current is confined in the resonant circuit. One possible modulation strategy of the converter is described in Fig. 3, which is explained thoroughly in [1]. It utilizes injection and free-wheeling oscillation during maximum absolute value of the three-phase input or,

$$\mathrm{Max}(v) = \max(|v_\mathrm{a}(t)|, |v_\mathrm{b}(t)|, |v_\mathrm{c}(t)|). \qquad (1)$$

Injection is used to increase the resonant current amplitude, while the free-wheeling is applied to reduce the amplitude. The indefinite operation involving injection and free-wheeling commutations will be called a normal mode in following sections. Fig. 3 also illustrates the operation during $\mathrm{Max}(v) = v_\mathrm{b}(t)$. It shows that the transition between injection and free-wheeling is performed at the zero-crossing of primary resonant current $i_\mathrm{p}(t)$ [1].

III. Initial Injection Method

To boost primary resonant current during initial operation of the AC/AC converter, the primary resonant capacitor is charged gradually during positive and negative phases of three-phase input until its voltage reaches a certain level. The level must be able to produce a sufficient initial current amplitude for a current transducer used in practical application. The process of capacitor

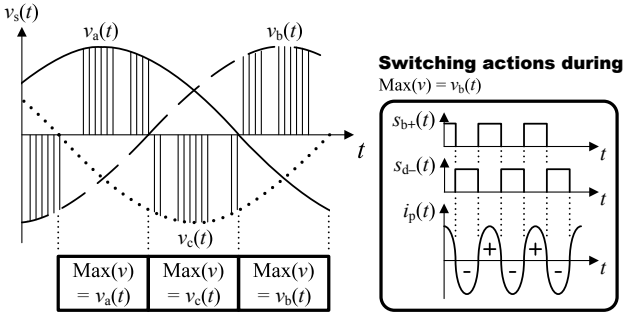

Fig. 3: A modulation strategy of ICPT system. Zero-current switching is performed to reduce switching power losses.

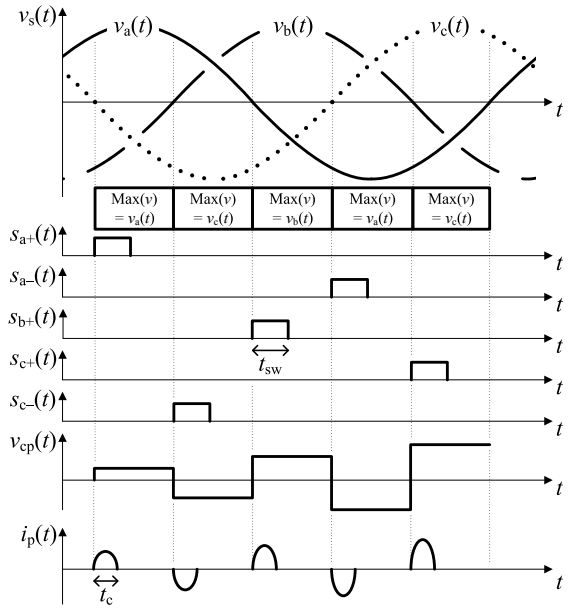

Fig. 4: Gradual capacitor charging mode of ICPT system. The pulse amplitude of $i_\mathrm{p}(t)$ is increased over time during the charging process.

charging is illustrated in Fig. 4. It shows positions of switching signals with respect to the three-phase input. The involved switches are turned-on at the beginning of $\mathrm{Max}(v)$ described in (1) and turned off after t_sw duration. The time has to be larger than a charging time t_c of

the resonant capacitor. Alternating polarity order must be used to increase the capacitor voltage. Therefore from Fig. 4, the switching order is Sa+, Sc−, Sb+, Sa− and Sc+ that corresponds to five cycles charging. It can be seen that Sd+ and Sd− that are responsible to free-wheeling commutation are not used in this case. When the pulse of $i_{\mathrm{p}}(t)$ is high enough to be read by the current transducer, the converter will start its normal operation, as was illustrated in Fig. 3.

A. Dynamic analysis

To calculate the charging voltage and current at the primary resonant capacitor, as well as the initial current boost due to the voltage, a dynamic analysis is needed. The dynamic equations will be obtained through a state-space approach. Equivalent representation of primary and secondary resonant circuits for modeling purpose is presented in Fig. 5. The schematic is based on one input phase, but can also be applied to the other two. The anti-parallel diode $\mathrm{D_{xy}}$ is always in the direction of the charging current $i_{\mathrm{p}}(t)$. Primary capacitor is labeled by C_{p}, while R_{p} and R_{s} are resistances of primary and secondary coils L_{p} and L_{s} respectively. The circuit is connected to a sampled voltage $v_{\mathrm{s}}(t)$ at the beginning of Max(v), which is denoted by $v_{\mathrm{in}}(t)$. Current on the secondary circuit is denoted by $i_{\mathrm{s}}(t)$. The battery is assumed to be purely resistive (R_{L}) and connected to a passive rectifier. Variable R_{eq} is a combination of the rectifier and R_{L} load obtained from [12]. All components are assumed to be ideal.

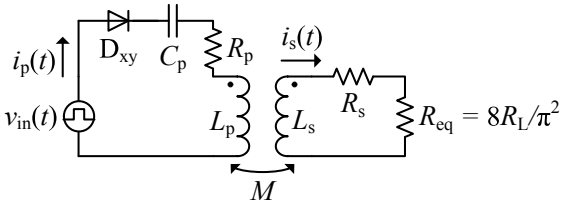

Fig. 5: Equivalent circuit of ICPT system that illustrates positive charging process. During negative charging, the diode $\mathrm{D_{xy}}$ and current $i_{\mathrm{p}}(t)$ are facing an opposite direction.

State-space representation of the converter can be obtained through manipulating dynamic equations based on circuit given in Fig. 5. The equation set is as follows,

$$\begin{cases} \dot{v_{\mathrm{cp}}}(t) = \dfrac{i_{\mathrm{p}}(t)}{C_{\mathrm{p}}}, \\ v_{\mathrm{in}}(t) = v_{\mathrm{cp}}(t) + i_{\mathrm{p}}(t)R_{\mathrm{p}} + L_{\mathrm{p}}\dot{i_{\mathrm{p}}}(t) - M\dot{i_{\mathrm{s}}}(t), \\ 0 = i_{\mathrm{s}}(t)(R_{\mathrm{s}} + R_{\mathrm{eq}}) + L_{\mathrm{s}}\dot{i_{\mathrm{s}}}(t) - M\dot{i_{\mathrm{p}}}(t), \end{cases} \tag{2}$$

where M is a mutual inductance between primary and secondary circuit that equals to $k\sqrt{L_{\mathrm{p}}L_{\mathrm{s}}}$. Variable k is a coupling factor between the primary and secondary sides.

The last two equations in (2) are combined to produce,

$$\dot{i_{\mathrm{p}}}(t) = \frac{1}{L_{\mathrm{p}}L_{\mathrm{s}} - M^2}\Big[L_{\mathrm{s}}v_{\mathrm{in}}(t) - L_{\mathrm{s}}v_{\mathrm{cp}}(t) - R_{\mathrm{p}}L_{\mathrm{s}}i_{\mathrm{p}}(t) - M(R_{\mathrm{s}} + R_{eq})i_{\mathrm{s}}(t)\Big], \tag{3}$$

$$\dot{i_{\mathrm{s}}}(t) = \frac{1}{L_{\mathrm{p}}L_{\mathrm{s}} - M^2}\Big[Mv_{\mathrm{in}}(t) - Mv_{\mathrm{cp}}(t) - MR_{\mathrm{p}}i_{\mathrm{p}}(t) - L_{\mathrm{p}}(R_{\mathrm{s}} + R_{\mathrm{eq}})i_{\mathrm{s}}(t)\Big]. \tag{4}$$

The first equation in (2), as well as equation (3) and (4) are joined to produce a state-space representation,

$$\begin{bmatrix} \dot{v_{\mathrm{cp}}}(t) \\ \dot{i_{\mathrm{p}}}(t) \\ \dot{i_{\mathrm{s}}}(t) \end{bmatrix} = \mathbf{A}\begin{bmatrix} v_{\mathrm{cp}}(t) \\ i_{\mathrm{p}}(t) \\ i_{\mathrm{s}}(t) \end{bmatrix} + \mathbf{B}v_{\mathrm{in}}(t),$$

$$\mathbf{A} = \begin{bmatrix} 0 & \frac{1}{C_{\mathrm{p}}} & 0 \\ -\frac{L_{\mathrm{s}}}{L_{\mathrm{p}}L_{\mathrm{s}}-M^2} & -\frac{R_{\mathrm{p}}L_{\mathrm{s}}}{L_{\mathrm{p}}L_{\mathrm{s}}-M^2} & -\frac{M(R_{\mathrm{s}}+R_{\mathrm{eq}})}{L_{\mathrm{p}}L_{\mathrm{s}}-M^2} \\ -\frac{M}{L_{\mathrm{p}}L_{\mathrm{s}}-M^2} & -\frac{MR_{\mathrm{p}}}{L_{\mathrm{p}}L_{\mathrm{s}}-M^2} & -\frac{L_{\mathrm{p}}(R_{\mathrm{s}}+R_{\mathrm{eq}})}{L_{\mathrm{p}}L_{\mathrm{s}}-M^2} \end{bmatrix}, \tag{5}$$

$$\mathbf{B} = \begin{bmatrix} 0 \\ \frac{L_{\mathrm{s}}}{L_{\mathrm{p}}L_{\mathrm{s}}-M^2} \\ \frac{M}{L_{\mathrm{p}}L_{\mathrm{s}}-M^2} \end{bmatrix}.$$

The representation can be solved through the Laplace transform approach explained in [13],

$$\begin{bmatrix} v_{\mathrm{cp}}(t) \\ i_{\mathrm{p}}(t) \\ i_{\mathrm{s}}(t) \end{bmatrix} = e^{\mathbf{A}t}\begin{bmatrix} v_{\mathrm{cp}}(0) \\ i_{\mathrm{p}}(0) \\ i_{\mathrm{s}}(0) \end{bmatrix} + \int_0^t e^{\mathbf{A}(t-\tau)}\mathbf{B}v_{\mathrm{in}}(\tau)d\tau, \tag{6}$$

$$e^{\mathbf{A}t} = \mathcal{L}^{-1}[(\mathrm{s}\mathbf{I} - \mathbf{A})^{-1}].$$

The charging voltage and current expressions are taken from the first and second rows of the solution. The capacitor voltage and charging current equations are given in (7) and (8),

$$v_{\mathrm{cp}}(t) = \phi_1(t)v_{\mathrm{cp}}(0) + \int_0^t \Big[\frac{\phi_2(t-\tau)L_{\mathrm{s}}}{L_{\mathrm{p}}L_{\mathrm{s}} - M^2} + \frac{\phi_3(t-\tau)M}{L_{\mathrm{p}}L_{\mathrm{s}} - M^2}\Big]v_{\mathrm{in}}(\tau)d\tau, \tag{7}$$

$$i_{\mathrm{p}}(t) = \phi_4(t)v_{\mathrm{cp}}(0) + \int_0^t \Big[\frac{\phi_5(t-\tau)L_{\mathrm{s}}}{L_{\mathrm{p}}L_{\mathrm{s}} - M^2} + \frac{\phi_6(t-\tau)M}{L_{\mathrm{p}}L_{\mathrm{s}} - M^2}\Big]v_{\mathrm{in}}(\tau)d\tau, \tag{8}$$

$$\phi_n(t) = \frac{\alpha_n s_1^2 + \beta_n s_1 + \gamma_n}{(s_1 - s_2)(s_1 - s_3)}e^{s_1 t} + \frac{\alpha_n s_2^2 + \beta_n s_2 + \gamma_n}{(s_2 - s_1)(s_2 - s_3)}e^{s_2 t} + \frac{\alpha_n s_3^2 + \beta_n s_3 + \gamma_n}{(s_3 - s_1)(s_3 - s_2)}e^{s_3 t} \tag{9}$$

$$\alpha_1 = 1,\ \ \beta_1 = \frac{R_\mathrm{p}L_\mathrm{s} + L_\mathrm{p}(R_\mathrm{s} + R_\mathrm{eq})}{L_\mathrm{p}L_\mathrm{s} - M^2},$$
$$\gamma_1 = \frac{R_\mathrm{p}(R_\mathrm{s} + R_\mathrm{eq})}{L_\mathrm{p}L_\mathrm{s} - M^2}, \tag{10}$$

$$\alpha_2 = 0,\ \ \beta_2 = \frac{1}{C_\mathrm{p}},\ \ \gamma_2 = \frac{1}{C_\mathrm{p}}\left[\frac{L_\mathrm{p}(R_\mathrm{s} + R_\mathrm{eq})}{L_\mathrm{p}L_\mathrm{s} - M^2}\right], \tag{11}$$

$$\alpha_3 = 0,\ \ \beta_3 = 0,\ \ \gamma_3 = -\frac{1}{C_\mathrm{p}}\left[\frac{M(R_\mathrm{s} + R_\mathrm{eq})}{L_\mathrm{p}L_\mathrm{s} - M^2}\right], \tag{12}$$

$$\alpha_4 = 0,\ \ \beta_4 = -\frac{L_\mathrm{s}}{L_\mathrm{p}L_\mathrm{s} - M^2},\ \ \gamma_4 = -\frac{R_\mathrm{s} + R_\mathrm{eq}}{L_\mathrm{p}L_\mathrm{s} - M^2}, \tag{13}$$

$$\alpha_5 = 1,\ \ \beta_5 = \frac{L_\mathrm{p}(R_\mathrm{s} + R_\mathrm{eq})}{L_\mathrm{p}L_\mathrm{s} - M^2},\ \ \gamma_5 = 0, \tag{14}$$

$$\alpha_6 = 0,\ \ \beta_6 = -\frac{M(R_\mathrm{s} + R_\mathrm{eq})}{L_\mathrm{p}L_\mathrm{s} - M^2},\ \ \gamma_6 = 0. \tag{15}$$

Variable s_1, s_2 and s_3 are roots of $\det(\mathrm{s}\mathbf{I} - \mathbf{A}) = 0$. Initial values of $i_\mathrm{p}(0)$ and $i_\mathrm{s}(0)$ are always zero in this case since the diode $\mathrm{D_{xy}}$ does not allow the current to oscillate (see Fig. 4). Thus the charging voltage value must be calculated at $t = t_\mathrm{c}$. For the charging current case, the value is taken at an extremum point. A comprehensive dynamic equation derivation of the converter can be found in [2].

The process of capacitor charge release to boost the initial current involves connecting the charged capacitor to one of the three-phase source. The capacitor and the source must have a different polarity. The process is slightly different than the charging itself since the current is allowed to oscillate after this point. To calculate the current amplitude, the charging current expression from (8) can be used. The value can be obtained by inserting a final charging voltage as an initial capacitor voltage $v_\mathrm{cp}(0)$. The current amplitude calculation is similar to the charging current calculation of the capacitor with an additional cycle. In other words, for two cycles charging voltage level, the converter will produce a current similar to a charging current of three cycles at the charge release.

B. Steady-state analysis

To simplify the dynamic analysis, two more assumptions are used, which are: the coupling between primary and secondary sides is loose, and the primary current distortion due to a damping effect is minimum. In this case, the charging time t_c can be approximated by a half of the system's resonant period. The coupled system resonant frequency is calculated through combining two steady-state equations as follows,

$$\begin{cases} \mathbf{V_{in}} = \dfrac{\mathbf{i_p}}{\mathrm{j}\omega C_\mathrm{p}} + \mathbf{i_p}\mathrm{j}\omega L_\mathrm{p} + \mathbf{i_p}R_\mathrm{p} - \mathbf{i_s}\mathrm{j}\omega M, \\ 0 = \mathbf{i_s}R_\mathrm{eq} + \mathbf{i_s}\mathrm{j}\omega L_\mathrm{s} + \mathbf{i_s}R_\mathrm{s} - \mathbf{i_p}\mathrm{j}\omega M, \end{cases} \tag{16}$$

variable $\mathbf{V_{in}}$ is an input of the resonant circuit. The combination of two steady-state equations in (16) by eliminating $\mathbf{i_s}$ leads to,

$$\mathbf{V_s} = \mathbf{i_p}\left[R_\mathrm{p} + \frac{\omega^2 M^2(R_\mathrm{eq} + R_\mathrm{s})}{\omega^2 L_\mathrm{s}^2 + (R_\mathrm{eq} + R_\mathrm{s})^2} + \mathrm{j}\left(\omega L_\mathrm{p} - \frac{1}{\omega C_\mathrm{p}} - \frac{\omega^3 M^2 L_\mathrm{s}}{\omega^2 L_\mathrm{s}^2 + (R_\mathrm{eq} + R_\mathrm{s})^2}\right)\right]. \tag{17}$$

During resonance ($\omega = \omega_0$), the imaginary part in (17) equals to zero,

$$\omega_0 L_\mathrm{p} - \frac{1}{\omega_0 C_\mathrm{p}} = \frac{\omega_0^3 M^2 L_\mathrm{s}}{\omega_0^2 L_\mathrm{s}^2 + (R_\mathrm{eq} + R_\mathrm{s})^2}, \tag{18}$$

$$C_\mathrm{p}(L_\mathrm{p}L_\mathrm{s}^2 - M^2 L_\mathrm{s})\omega_0^4 + [L_\mathrm{p}C_\mathrm{p}(R_\mathrm{eq} + R_\mathrm{s})^2 - L_\mathrm{s}^2]\omega_0^2 - (R_\mathrm{eq} + R_\mathrm{s})^2 = 0, \tag{19}$$

which has a biquadratic form. Four roots can be calculated through the quadratic formula. One root that has positive and real value is the resonant frequency ω_0. The equation is described as follows,

$$\omega_0 = \pm\sqrt{-\mathrm{A} \pm \Omega}, \tag{20}$$

$$\mathrm{A} = \frac{1}{2L_\mathrm{p}^2}\left[\frac{m^2(R_\mathrm{eq} + R_\mathrm{s})^2 - n}{1 - k^2}\right], \tag{21}$$

$$\Omega = \sqrt{\mathrm{A}^2 + \frac{nm^2(R_\mathrm{eq} + R_\mathrm{s})^2}{L_\mathrm{p}^4(1 - k^2)}}, \tag{22}$$

$$m = \frac{L_\mathrm{p}}{L_\mathrm{s}}, \quad n = \frac{L_\mathrm{p}}{C_\mathrm{p}}. \tag{23}$$

The resonant period is $T_0 = 2\pi/\omega_0$. The charging voltage and maximum primary current amplitude can be approximated at $T_0/2$ and $T_0/4$ respectively.

C. Analytical calculation

For an initial prototype, the ICPT system is designed to deliver power less than 1 kW. Parameter values for the circuit are given in TABLE I. Resonant circuit quantities are based on components selection given in [2]. The selection results keep a damping ratio of the primary resonant current under a certain level. The ratio permits the current to keep oscillating during converter operation. Load values R_L and R_eq are based on [3] to minimize coils' power losses. Switching frequency of the converter is the same as a resonant frequency of the coupled resonant circuit. The value depends on the coupling factor and load conditions.

During one cycle charging process, the input voltage $v_\mathrm{in}(t)$ is assumed to be constant since the charging time is much smaller than the input three-phase period. The voltage value is sampled at the beginning of $\mathrm{Max}(v)$ (see Fig. 4) which is equal to $\pm V_\mathrm{s}\sin(\pi/3)$, where V_s is the amplitude of $v_\mathrm{s}(t)$. Positive and negative symbol indicates that the voltage source is taken from either positive or negative source, depending on the resonant capacitor voltage state. In a case of an input source with 100 V peak voltage, the value of $v_\mathrm{in}(t)$ becomes $\pm$86.603 V. By using the MATLAB software, capacitor voltage, as

well as charging and produced currents of the circuit are calculated and given in TABLE II. Variable V_{cp} and I_p are amplitude or extremum value. The voltage is calculated at $T_0/2$, while the current is at $T_0/4$. The calculated resonant frequency is 26.983 kHz for $k = 0.55$ and $R_L = 47.742\ \Omega$. And for $k = 0.83$ and $R_L = 58.708\ \Omega$, the frequency is 29.139 kHz.

IV. Simulation Results

The given values in TABLE I are used in a simulation model of the ICPT system built using the PLECS software. All simulation results are obtained when the system is in an open-loop configuration.

A. Initial injection without gradual charging

Without gradual charging, initial capacitor voltage is zero, and resonant current is increased through injection and free-wheeling commutations. In other words, the converter is operating in a normal mode immediately as was shown in Fig. 3. Simulation results for two different coupling factors and loads are given in Fig. 6. Parameters $v_a(t)$, $v_b(t)$ and $v_c(t)$ indicate phase-A, B and C of the three-phase input while $v_{res}(t)$ is a voltage over the primary resonant circuit. The current $i_p(t)$ in this case is the primary resonant current. Initial current amplitudes (marked by red circles) produced by applying voltage over the resonant circuit are approximately 2.721 A for $k = 0.55$ and 2.544 A for $k = 0.83$. Switching of Sa+ gate begins at the beginning of $\text{Max}(v) = v_a(t)$.

It can be seen that Sa+ is starting initial current injection directly from input phase-A. With the CASR-6 current transducer described in [9], its output will be 0.289 V for 2.721 A and 0.27 V for 2.544 A, around 2.5 V offset voltage. The values may be too small for a practical comparator-based zero-crossing detector, that is connected directly to its output.

B. Initial injection with gradual charging

In this case, the initial current is increased with a help of primary capacitor voltage that has been charged to a certain level. As examples, two cycles charging were performed on the simulation model and the results are given in Fig 7 and 8. Each result corresponds to a certain combination of coupling factor and load. The

TABLE I: PARAMETER VALUES

Symbol	Meaning	Value
V_s	Line voltage amplitude	100 V
f	Line voltage frequency	50 Hz
C_p	Primary capacitance	0.2 μF
L_p	Primary inductance	0.2 mH
L_s	Secondary inductance	0.2 mH
k	Coupling factor	$0.55 - 0.83$
R_p	Primary coil resistance	0.3 Ω
R_p	Secondary coil resistance	0.3 Ω
R_L	Load resistance	$47.742 - 58.708\ \Omega$
R_{eq}	Equivalent load resistance	$38.698 - 47.587\ \Omega$

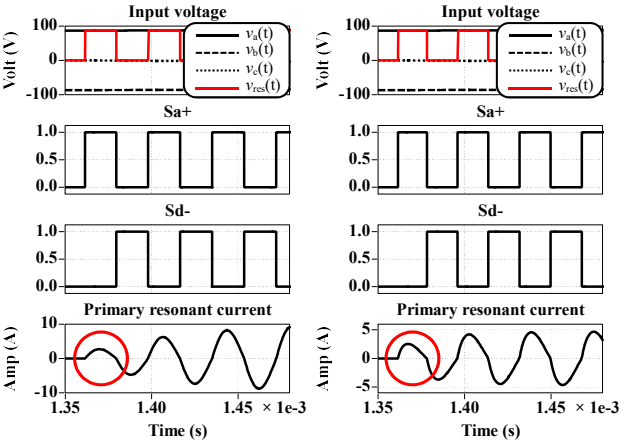

Fig. 6: Simulation results of initial transient without gradual charging with time range $1.35 - 1.48$ ms. Left graph corresponds to k = 0.55 and R_L = 47.742 Ω, while the right one relates to k = 0.83 and R_L = 58.708 Ω. Red circles indicate first current injection.

charging process happens around $t < 8$ ms. The primary capacitor is gradually charged twice at the beginning of two $\text{Max}(v)$ with a different source polarity consecutively. The quantities of both figures are presented in TABLE III and IV.

In Fig. 7, the capacitor voltage is charged to approximately -284.57 V, and in 8 is up to around -216.378 V, before they are used to boost the initial primary resonant current. Fig. 8 is a tighter coupling case compared to Fig. 7. The charging are performed twice at the beginning of $\text{Max}(v) = v_a(t)$ and $\text{Max}(v) = v_c(t)$. Voltage over the resonant circuit is indicated by $v_{res}(t)$ on the first plot of each figure. This voltage is equal to the capacitor voltage $v_{cp}(t)$ during the charging process. The IGBT that is responsible for charging in both cases are conducted for 1 ms, which is longer than the system's resonant period which is in a range of $34.318\ \mu s \leq t_c \leq 37.06\ \mu s$. By

TABLE II: CALCULATION RESULTS

	$k = 0.55$, $R_L = 47.742\Omega$		$k = 0.83$, $R_L = 58.708\Omega$	
Charging cycle	Capacitor voltage (V_{cp})	Charging current (I_p)	Capacitor voltage (V_{cp})	Charging current (I_p)
1	156.9 V	2.678 A	137.199 V	2.283 A
2	-284.065 V	-7.532 A	-217.061 V	-5.899A
3	387.130 V	11.465 A	263.547 V	8.004 A
4	-470.662 V	-14.653 A	-290.606 V	-9.229 A
5	538.363 V	17.237 A	306.357 V	9.942 A

TABLE III: SIMULATION RESULTS 1

$k = 0.55$, $R_L = 47.742\ \Omega$		
Charging cycle	Capacitor voltage (V_{cp})	Charging current (I_p)
1	157.12 V	2.72 A
2	-284.57 V	-7.65 A

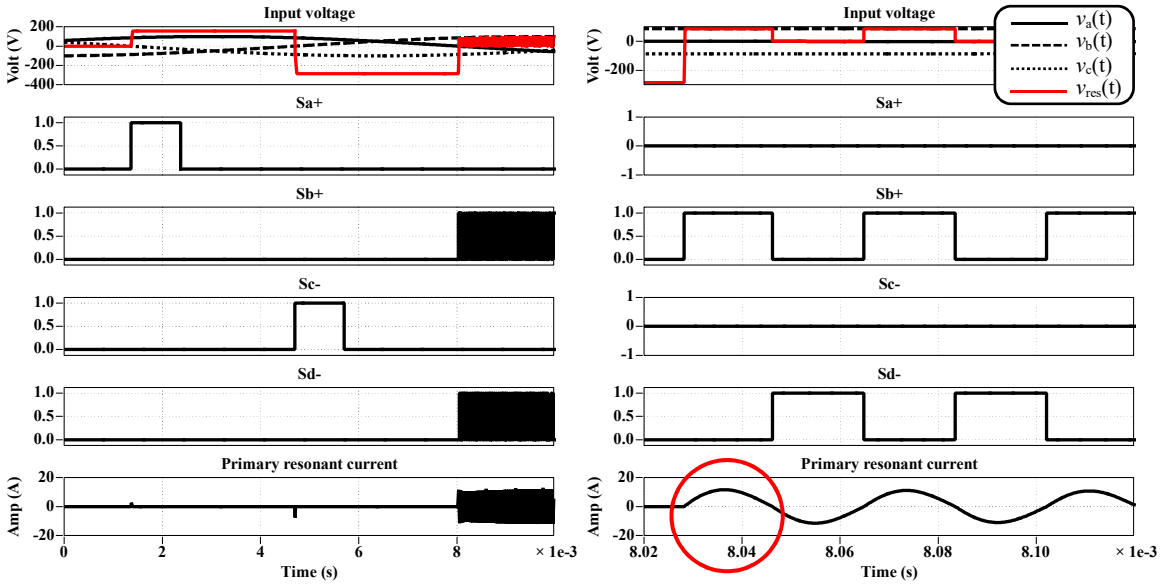

Fig. 7: Simulation result of initial transient using gradual charging for k = 0.55 and R_L = 47.742 Ω. The right graph is a zoomed version of the left around 8 ms time axis. Left graph has a timescale of $1-10$ ms, while the right one has $8.02-8.12$ ms. Red circle indicates first current injection.

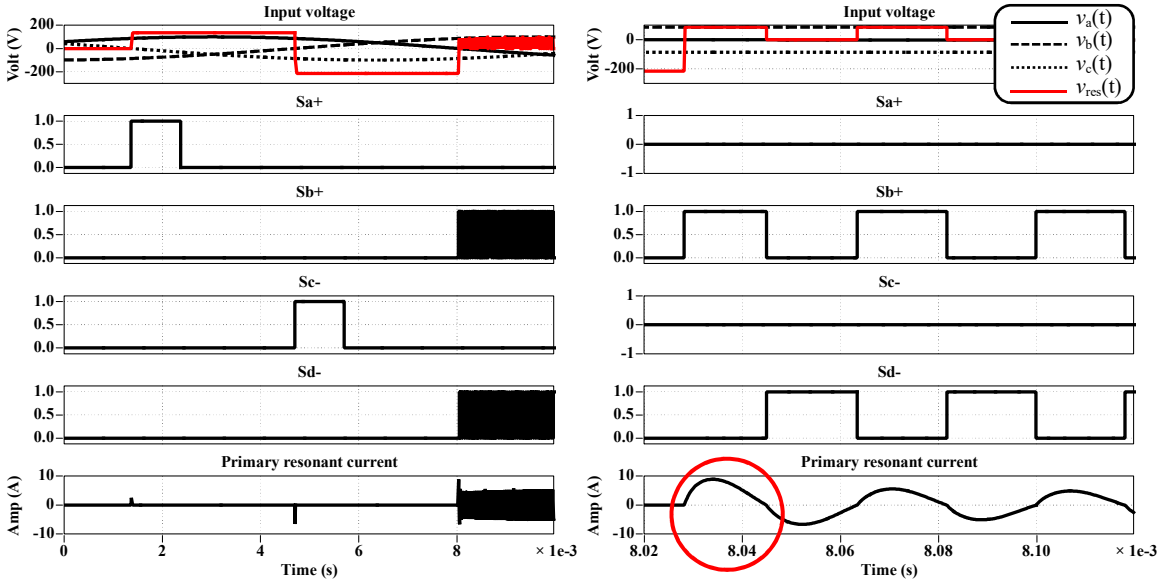

Fig. 8: Simulation result of initial transient using gradual charging for k = 0.83 and R_L = 58.708 Ω. The right graph is a zoomed version of the left around 8 ms time axis. Left graph has a timescale of $1-10$ ms, while the right one has $8.02-8.12$ ms. Red circle indicates first current injection.

TABLE IV: SIMULATION RESULTS 2

$k = 0.83$, $R_L = 58.708$ Ω

Charging cycle	Capacitor voltage (V_{cp})	Charging current (I_p)
1	137.01 V	2.545 A
2	-216.378 V	-6.565 A

comparing simulation and analytical results (TABLE II, III and IV), it can be seen that they are similar. In both figures, the first current injection amplitude is 11.651 A for $k = 0.55$ and 8.895 A for $k = 0.83$. If CASR-6 is used, then its output voltage will be 1.238 V and 0.945 V respectively which are big enough to be distinguished by a comparator-based zero-crossing detector [9]. Both injection currents are also similar to the charging current of the three charging cycles for each particular case (see TABLE II).

By observing current waveforms inside red circles in both Fig. 7 and 8, a higher coupling factor leads to a deformed sinusoidal current waveform. The deformation

is caused by a higher damping ratio which is explained further in [2]. This effect can cause analytical calculations that utilizes the resonant frequency less accurate.

V. Conclusion

An initial injection method of a direct AC/AC converter for inductive charger has been demonstrated at a simulation level. It is based on a DC resonant charging by taking advantage of converter topology. The purpose is to increase amplitude of initial current injection in a primary resonant circuit, without adding output amplification on a used current transducer. This method is useful due to limited measurement range of an affordable current transducer and the existence of measurement noise. Analytical calculation to predict charging behavior was verified by the simulation results. It has to be noted that the calculation approach is more accurate for a loosely coupled system. Experimental setup is currently being built that will demonstrate the performance of the circuit as well as its initial charging method.

References

[1] F. P. Kusumah *et al.*, "A Direct Three-Phase to Single-Phase AC/AC Converter for Contactless Electric Vehicle Charger," in *Proc. European Conference on Power Electronics and Applications*, Geneva, 2015, pp. 1-10.

[2] F. P. Kusumah *et al.*, "Components Selection of a Direct Three-Phase to Single-Phase AC/AC Converter for Contactless Electric Vehicle Charger," in *Proc. European Conference on Power Electronics and Applications*, Karlsruhe, 2016, pp. 1-10.

[3] F. P. Kusumah and J. Kyyrä, "Minimizing Coil Power Loss in a Direct AC/AC Converter-based Contactless Electric Vehicle Charger," in *Proc. European Conference on Power Electronics and Applications*, Warsaw, 2017, pp. 1-10.

[4] N. X. Bac et al., "A Matrix Converter Based Inductive Power Transfer System," in *Proc. International Power and Energy Conference*, Dec 2012, pp. 509-514.

[5] N. X. Bac et al., "A SiC-Based Matrix Converter Topology for Inductive Power Transfer System," *IEEE Transactions on Power Electronics*, vol. 29, issue 8, pp. 4029-4038.

[6] A. P. Hu and Hao L. Li, "A new high frequency current generation method for inductive power transfer applications," in *Proc. IEEE Power Electronics Specialists Conference*, Jeju, 2006, pp. 1-6.

[7] Li, Hao L. *et al.*, "FPGA Controlled High Frequency Resonant Converter for contactless Power Transfer," in *Proc. IEEE Power Electronics Specialists Conference*, Rhodes, 2008, pp. 3642-3647.

[8] Hao Leo Li *et al.*, "A Direct AC-AC Converter for Inductive Power-Transfer Systems," in *IEEE Transactions on Power Electronics*, vol. 27, pp. 661-668, Jun 2011.

[9] LEM. (2017, October 23). *Current transducer CASR series* [Online]. Available: http://www.lem.com/docs/products/casr_series.pdf

[10] P. Horowitz and W. Hill, *The Art of Electronics*, 3rd ed. New York, USA: Cambridge University Press, 2015.

[11] H. J. White *et al.*, "THE CHARGING CIRCUIT OF THE LINE-TYPE PULSER," in *PULSE GENERATORS*. New York, NY: Dover, 1948.

[12] R. L. Steigerwald, "A Comparison of Half-Bridge Resonant Converter Topologies," in *IEEE Transactions on Power Electronics*, vol. 3, pp. 174-182, Apr 1988.

[13] Katsuhiko Ogata, "Control Systems Analysis in State Space," in *Modern Control Engineering*, 5th ed., Upper Saddle River, NJ: Pearson Education, Inc., 2010, pp. 648-721.